Fully Dense Yttrium-Substituted Hydroxyapatite Coatings with Aligned Crystal Domains

ARTICLE *in* CRYSTAL GROWTH & DESIGN · DECEMBER 2011

Impact Factor: 4.89 · DOI: 10.1021/cg200943s

4 AUTHORS, INCLUDING:

Xue Wei
Greatbatch Medical
6 PUBLICATIONS **28** CITATIONS
SEE PROFILE

Cong Fu
University of Rochester
10 PUBLICATIONS **41** CITATIONS
SEE PROFILE

CRYSTAL GROWTH & DESIGN

ARTICLE

pubs.acs.org/crystal

Fully Dense Yttrium-Substituted Hydroxyapatite Coatings with Aligned Crystal Domains

Xue Wei, Cong Fu, Keith Savino, and Matthew Z. Yates*

Department of Chemical Engineering and Laboratory for Laser Energetics, 206 Gavett Hall, University of Rochester, Rochester, New York 14627, United States

ABSTRACT: Continuous yttrium-substituted hydroxyapatite (Y-HAP) coatings on titanium substrates were produced by an electrochemical/hydrothermal method. Hydroxyapatite seeds were first deposited on the titanium surface by electrochemical deposition. Subsequent hydrothermal crystal growth of Y-HAP onto the seed layer was investigated over a range of experimental conditions. Under certain conditions, it was discovered that well-crystallized and fully dense Y-HAP films were produced consisting of crystal domains oriented with the crystallographic *c*-axis normal to the substrate. At elevated temperatures, protons conduct along the *c*-axis of Y-HAP crystals. The novel film microstructure can therefore potentially be exploited in new applications of Y-HAP in bioelectrets, fuel cells, and electrochemical sensors.

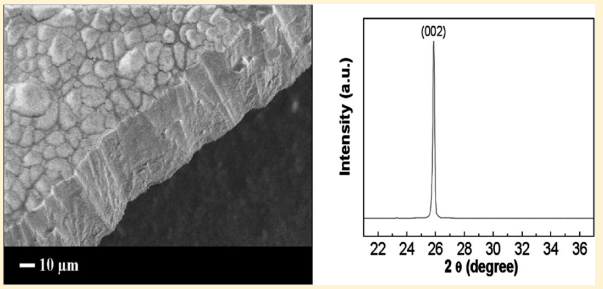

INTRODUCTION

Hydroxyapatite ($Ca_{10}(PO_4)_6(OH)_2$ or HAP) is similar in composition to naturally occurring apatites in teeth and bones, and is often coated onto biomedical implants to improve biocompatibility.[1] A variety of methods have been developed to coat HAP onto metal substrates, including sol−gel synthesis, electrochemical deposition, sputter coating, hydrothermal deposition, and electrophoretic deposition.[2−8] The most common substrates coated with HAP are titanium and stainless steel because they are used in load bearing orthopedic implants. The bioactivity of HAP strongly depends on mechanical and dissolution properties of coated films. Amorphous or poorly crystalline HAP films dissolve easily in vivo, or have poor adherence to the substrate.[6,7,9] Continuous and highly crystallized HAP films with good substrate adherence are preferable for improved durability and biocompatibility.

The crystallinity and crystal orientation of HAP can also significantly affect electrical properties of the coatings. High temperature electrochemical investigations reveal HAP to be a purely proton conducting material, with proton conductivity of 10^{-9}−10^{-7} S/cm from 500 −800 °C.[10−12] The mechanism of proton conductivity is thought to involve the shuttling of protons along hydroxyl groups that line the crystallographic *c*-axis.[13,14] At elevated temperatures, an applied electric field will cause HAP crystals to become polarized along the *c*-axis due to the field-induced movement of protons.[14] If the electric field is maintained as crystals are cooled, then the crystals will have permanent electrical polarization along the *c*-axis at room temperature. Numerous studies have shown that bone growth is improved on the negatively charged hydroxyapatite crystal surfaces of polarized crystals.[15−18]

The electrochemical properties of HAP suggest that it may also be effective as a proton-conducting electrolyte for fuel cells and other electrochemical devices. Measurements of high temperature electrical polarization and depolarization of HAP reveal an onset of proton mobility within the crystals at temperatures as low as 200−250 °C.[14] While protons are quite mobile along the *c*-axis of individual HAP crystals, the proton conductivity of bulk sintered HAP ceramics is relatively low.[10] There is evidence that boundaries between crystal domains act as traps for protons, lowering the overall conductivity.[10] We recently reported a novel approach to improve proton transport through HAP membranes by microstructural engineering.[19] The concept is analogous to the microstructural engineering of molecular sieve membranes to improve mass transport.[20] Our synthetic approach produced hydroxyapatite membranes consisting of aligned crystal domains with the c-axes spanning the membrane thickness. Thus, the ion transport path length is minimized and grain boundary resistance to ion transport is eliminated. The membranes with structure optimized for proton transport displayed proton conductivity nearly 4 orders of magnitude higher than traditional sintered ceramics of the same material.[19] The control of the coating's microstructure was achieved through multiple hydrothermal crystallization steps with surfactants added to alter the relative growth rates of the crystal *c*-axis versus *a*-axis. The seeded hydrothermal growth was found to produce dense, well-crystallized coatings on metal substrates.[21]

In the present study, we investigate the microstructural engineering of yttrium-doped hydroxyapatite (Y-HAP) coatings

Received: July 21, 2011
Revised: November 2, 2011
Published: November 10, 2011

on titanium. Yttrium doping has been shown to enhance osteoblast adhesion and calcium deposition onto hydroxyapatite coatings, indicating that Y-HAP may be preferable to pure HAP in improving the performance of orthopedic and dental implants.[22,23] The Y^{3+} ions substitute for Ca^{2+} in the crystal framework, causing the number of hydroxyl ions to decrease since OH^- is transformed to O^{2-} for electrical charge compensation. As a result, yttrium doping also significantly affects ion conduction at elevated temperatures. The chemical formula of Y-HAP is given by the following: $Ca_{10-x}Y_x(PO_4)_6(OH)_{2-x}O_x$ where "x" is the composition parameter for yttrium.[24] As x is increased from 0 to 0.65, the proton conductivity of bulk Y-HAP rises from $\sim 10^{-7}$ to $\sim 10^{-4}$ S/cm at 800 °C, while the activation energy for conduction falls from ~1.5 to ~1.0 eV.[25] At higher levels of yttrium doping, Y-HAP transitions from a pure proton conductor at $x = 0.65$ to a pure oxygen ion conductor at $x > 1$.[25,26] The transition to an oxygen ion conductor is accompanied by a fall in conductivity and rise in activation energy for ion conduction.

We recently reported the hydrothermal crystal growth of Y-HAP onto palladium substrates seeded with HAP nanocrystals.[27] During hydrothermal crystal growth, yttrium doping was found to provide the dual benefit of improving conductivity and promoting the formation of fully dense films with near perfect alignment of the crystallographic c-axis normal to the substrate. The resulting microstructure promotes proton transport through the membrane. Y-HAP films on palladium with the composition parameter $x \approx 0.65$ displayed the remarkably high proton conductivity of nearly 10^{-2} S/cm at 700 °C, which is comparable to many ceramic electrolytes used in fuel cells and other electrochemical devices.[27] Here, we report a more detailed study of hydrothermal crystal growth of Y-HAP onto titanium substrates to obtain fully dense coatings with the c-axis oriented normal to the substrate. The microstructure is ideal for electrically polarizing the crystals in the film with the dipole oriented normal to the surface. The novel Y-HAP coatings may display improved performance in dental and orthopedic implants, as well as in electrochemical devices.

EXPERIMENTAL SECTION

Materials. K_2HPO_4 (99.99% purity), $CaCl_2$ $2H_2O$ (99+% purity), NaCl (99.0% purity), tris(hydroxymethyl)-amino-methane (99.8+% purity), $Ca(NO_3)_2 \cdot 4H_2O$ (99.0% purity), and disodium ethylenediaminetetraacetate dihydrate ($Na_2EDTA \cdot 2H_2O$) (99.0−101.0% purity) were all obtained from Sigma-Aldrich. $(NH_4)_2HPO_4$ (>99.0% purity) was purchased EMD. 37% hydrochloric acid and 28.0−30.0% ammonium hydroxide were purchased from Mallinckrodt Chemicals. $Y(NO_3)_3 \cdot 6H_2O$ (99.9% purity), titanium (Ti) foil (0.89-mm thick), and platinum (Pt) foil (0.127-mm thick) were obtained from Alfa Aesar.

Sample Preparation and Characterization. HAP seeds were deposited onto the Ti substrate through the electrochemical deposition method.[4,19,28] In brief, a precleaned Ti plate (12.5 × 12.5 × 0.89 mm) was used as the cathode and the anode was a platinum plate (25 × 25 × 0.127 mm). The electrolyte solution consisted of 138 mM NaCl, 50 mM tris(hydroxymethyl)-aminomethane, 1.3 mM $CaCl_2$, 0.84 mM K_2HPO_4 in deionized water. The solution was buffered to pH 7.2 using 37% hydrochloric acid. The electrochemical reaction was carried out at ~95 °C for 5 min with constant current density of 12.5 mA/cm^2. After the deposition, the cathode electrode seeded with HAP crystals was taken out of the electrolyte solution, rinsed with deionized water several times, and dried in air.

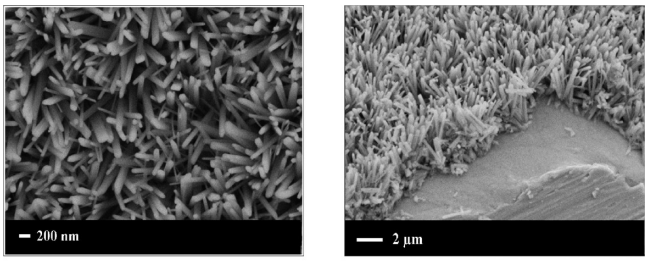

Figure 1. SEM images of HAP seeds on Ti substrate prepared by electrochemical deposition at 12.5 mA/cm^2 current for 5 min: (a) top-view and (b) side-view.

The seeded substrate was placed in a Teflon-lined vessel with the seed layer facing down and tilted up at about 45° relative to the bottom of the vessel. For a typical hydrothermal solution, Na_2EDTA (0.115 M) was first completely dissolved into 30 mL deionized water. $Ca(NO_3)_2$ (0.1 M), $Y(NO_3)_3$, (0.01 M), and $(NH_4)_2HPO_4$ (0.06 M) were successively added and the solution was stirred for 30 min. The salts, particularly nitrates, are very hygroscopic and should not be exposed to humid air. The solution was adjusted to pH = 10.0 with ammonium hydroxide and then transferred to the Teflon-lined vessel to immerse the seeded substrate. The Teflon-lined vessel was sealed in a stainless steel autoclave and put into a convective oven for hydrothermal synthesis at 200 °C for 15 h. After the reaction, the autoclave was cooled to room temperature in air. The sample was taken out, rinsed with deionized water several times, and dried in air. Morphology of the products was examined using a field emission source scanning electron microscope (FESEM, Zeiss-Leo DSM982). Some SEM images have brighter regions due to electrical charging because the samples were not sputter coated with metal prior to SEM analysis. Coating thickness was estimated by side view SEM images of fractured films. The reported thickness was an average of several measurements. ImageJ software was used to calculate the fraction of the top-view SEM image area occupied by crystals. An estimate of film porosity was obtained by assuming that the fraction of the film occupied by crystals is constant throughout the film volume. The crystal structure was determined by X-ray diffraction (XRD) (Philips PW3020) with Cu Kα radiation (λ=1.5418 Å) in the 2θ range from 20° to 40°. The crystallographic texture of HAP seeds and Y-HAP dense film was evaluated by pole figures of the (002) plane using a Philips Hi-Resolution X'PERT PRO X-ray diffractometer (PANalytical, Netherlands). The (002) peak intensity was measured at every 5 degrees of tilt angle, starting from 0° (normal to the substrate) to 85°. At each tilt angle, data were collected as the sample was rotated 360° azimuthally. In each plot, the intensity was normalized to the most intense peak. The intensity plots represent the distribution of (002) planes relative to the substrate surface. The strength of adhesion of the fully dense coating was qualitatively measured by the ASTM standard D3359 tape test.

RESULTS AND DISCUSSION

Seed crystal layers were deposited onto titanium through electrochemical deposition under conditions similar to those previously reported in the literature.[4,19,28] In the electrochemical process, a direct current is applied through the electrolyte solution containing dissolved calcium and phosphate. Hydroxyapatite nucleates on the surface of the metal cathode due to the accumulation of calcium ions by electrostatic attraction and the local increase in pH due to the electrolysis of water. Over long deposition times, hydrogen gas evolution on the cathode surface tends to dislodge deposited crystals, making coatings of uneven

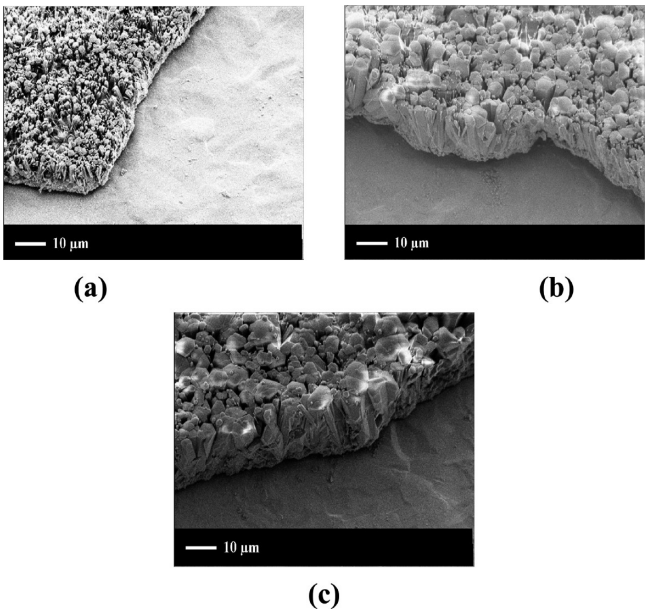

Figure 2. Side-view SEM images of Y-HAP coatings as a function of reaction time in the hydrothermal process: (a) 5 h, (b) 15 h, and (c) 30 h.

thickness.[21] To overcome this limitation of electrochemical deposition, the reaction was carried out for only a short period of time to ensure a uniform coating. Figure 1 shows the top-view and side-view of the HAP seed layer formed on the titanium substrate in 5 min at 95 °C with a constant current density of 12.5 mA/cm^2. The crystals in the seed layer typically have a needle-like morphology of ~1 to 2 μm in length and submicrometer width. The crystal morphology is consistent with previous reports of electrochemical deposition, and the longest axis of the rod-shaped crystals is associated with the crystallographic *c*-axis.

The deposited HAP seeds provided nucleation sites for subsequent hydrothermal crystal growth of Y-HAP into a dense crystalline film on the substrate. For hydrothermal crystallization, EDTA was added to the synthesis mixture in order to chelate the calcium and yttrium ions. The growth was carried out at 200 °C and pH = 10 with an aqueous solution of Ca-EDTA complex, Y-EDTA complex, ammonium phosphate and ammonium hydroxide to adjust solution pH. As the reaction mixture is heated, the EDTA complexes are broken down to release free calcium and yttrium cations. The free cations then react with ammonium phosphate to nucleate and grow Y-HAP. EDTA thus regulates supersaturation of Y-HAP in order to promote crystal growth onto the seeded surface and limit homogeneous nucleation in solution.[19] Figure 2 shows SEM images of Y-HAP hydrothermally grown on seeded titanium substrates. Figure 2(a) shows that the Y-HAP crystals grown for 5 h have a size of ~1 μm in width and ~7 μm in length. As the reaction time was increased to 15 h, the width of the crystals increased to ~5 μm and the length was increased to ~11 μm, as shown in Figure 2(b). Crystals grown for 30 h are similar in size to those prepared for 15 h, as shown in Figure 2(c). Extending the growth time to 45 h also produced crystals similar in size (not shown) to those produced after 15 h. The hydrothermal crystal growth onto the seeded substrate is initially rapid, but essentially stops beyond 15 h. In the beginning of the reaction, sufficient amount of reactants are available so that crystals grow longer and wider with time. As the

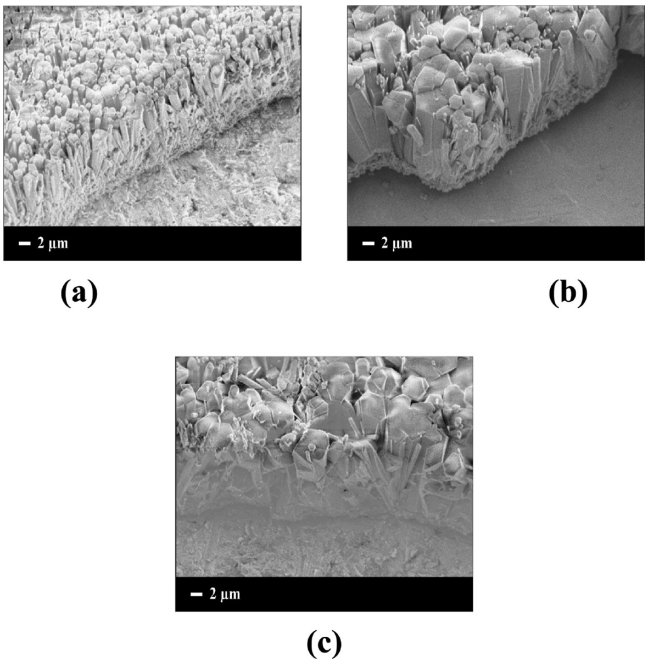

Figure 3. Side-view SEM images of hydrothermally crystallized Y-HAP coatings on titanium as a function of the initial pH: (a) pH = 8, (b) pH = 10, and (c) pH = 11.

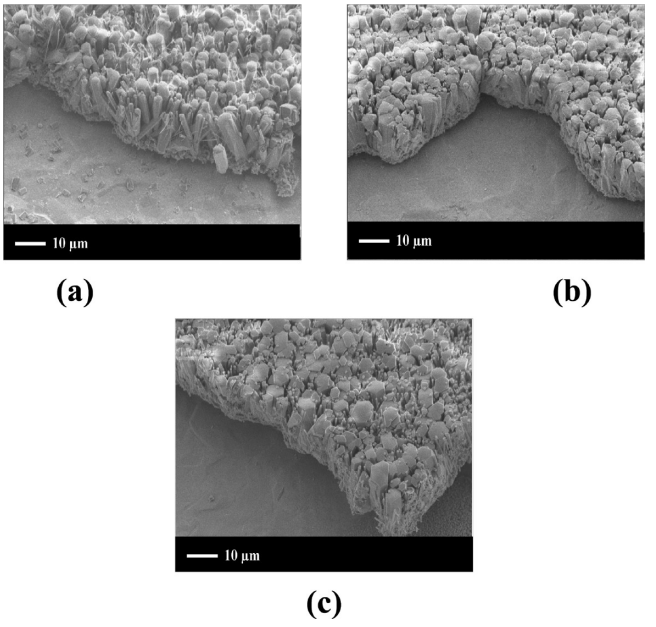

Figure 4. Side-view SEM images of Y-HAP coatings on titanium as a function of starting [Ca] in the hydrothermal process: (a) [Ca] = 0.05 M, (b) [Ca] = 0.1 M, and (c) [Ca] = 0.4 M.

reaction proceeds, crystal growth slows as reactants are depleted due to growth on the seeded substrate as well as homogeneous crystal nucleation from solution. On the basis of the results in Figure 2, a hydrothermal growth time of 15 h was chosen as a standard synthesis condition.

Figure 3 shows the effect of varying solution pH on the morphology of Y-HAP crystals grown on the seeded substrate for 15 h at 200 °C. It was found that the thickness and density of

dx.doi.org/10.1021/cg200943s |*Cryst. Growth Des.* 2012, 12, 217–223

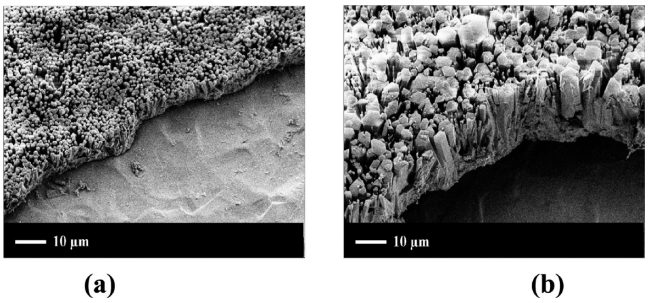

Figure 5. Side-view SEM images of Y-HAP coatings as a function of starting [P] in the hydrothermal process: (a) [P] = 0.03 M, (b) [P] = 0.09 M.

the Y-HAP coating both increased with increasing pH. Figure 3-(a) shows that the Y-HAP crystals in the coating have a size of ~1−2 μm in width and ~10 μm in length when pH was 8. As pH was increased to 10 and 11, the width of the crystals increased to ~5−7 μm, while the coating thickness increased to ~11 μm. The release of free calcium and yttrium from EDTA complexes is regulated by pH as well as temperature. As pH is increased, the dissolution of the EDTA complexes is slowed, which leads to less free calcium and yttrium ions.[8] In addition, the solubility of most apatites also decreases with increasing pH.[1,29] A more dense coating on the substrate is obtained as pH is increased, but a complete understanding of the factors responsible for morphological changes in the film would require determination of speciation of all compounds under the experimental conditions.

The influence of calcium concentration on the Y-HAP crystal morphology produced at 200 °C for 15 h at pH = 10 is shown in Figure 4. The starting calcium concentration was varied from 0.05, 0.1, and 0.4 M, while the yttrium concentration was fixed at 0.01 M and phosphate concentration was fixed at 0.06 M. To fully complex the calcium added, the amount of EDTA was adjusted according to the equation: [EDTA] = [Ca] + 1.5[Y]. The cross-sectional SEM images reveal that the thickness of the coatings decreases slightly while the density increases significantly as calcium concentration is raised. When the starting calcium concentration is 0.05 M, the coating thickness is around 12 μm and many gaps between crystals are observed to extend down to the bottom of the coating. As the calcium concentration was increased to 0.4 M, most crystal domains grew together to form a dense film with a thickness of 10 μm. The side view image in Figure 4(c) shows the gaps between crystal domains on the upper surface do not extend throughout the film.

Studies of hydroxyapatite as a liquid chromatography packing have shown that the crystal facets parallel to the c-plane (or c-surfaces) are negatively charged while those parallel to the (a, b) plane (or a-surfaces) are positively charged.[30,31] Since a small fraction of Y substitution does not affect the structure of HAP crystals due to the similar size of Y^{3+} and Ca^{2+}, we postulate the surface charges of Y-HAP facets are similar to that of HAP. It is expected that the positively charged calcium ions are preferentially absorbed to the negative charged c-surfaces. When a nonreactive molecule or ion preferentially adsorbs onto one facet of a growing crystal, it lowers the interfacial free energy of that facet, and the crystal growth onto that facet is slowed relative to others.[32,33] However, calcium also participates in the crystal growth reaction so that increasing calcium concentration can promote lateral intergrowth of crystals along the *a*-axis to

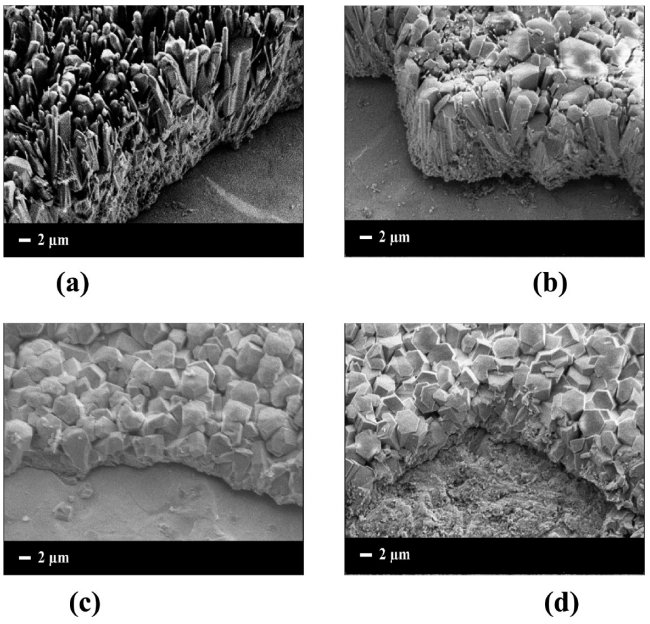

Figure 6. Side-view SEM images of Y-HAP coatings as a function of starting [Y] in the hydrothermal process: (a) No Y, (b) [Y] = 0.0067 M, (c) [Y] = 0.02 M, and (d) [Y] = 0.05 M.

produce a dense coating as a result of an increase in local supersaturation.

The effect of phosphate concentration on the Y-HAP coatings was investigated by varying the initial phosphate concentration from 0.03 and 0.09 M, while the concentration of calcium was held constant at 0.1 M and yttrium held constant at 0.01 M. As shown in Figure 5, increasing phosphate concentration results in thicker films consisting of larger crystals. With 0.03 M phosphate, the crystal width and length in the coatings were around 1 and 5 μm, respectively. Increasing in the phosphate concentration to 0.09 M produced crystals ~6 μm in width, while the length was increased to ~15 μm. It is expected that the negatively charged phosphate ions preferentially adsorb onto the positively charged a-surfaces. As a result, high phosphate concentration tends to form crystals with longer *c*-axis. Since the *c*-axis is preferentially oriented normal to the surface, the thickness of the films is increased.

A series of experiments were carried out with varying initial yttrium concentration while holding calcium concentration fixed at 0.1 M, and phosphate concentration fixed at 0.06 M. Again, the EDTA concentration was adjusted to ensure complete complexation of the cations according to the formula: [EDTA] = [Ca] + 1.5[Y]. A control experiment without the yttrium salt was also performed. After hydrothermal crystal growth for 15 h at 200 °C, homogeneous coatings of relatively uniform thickness were obtained for all samples. Without yttrium addition, HAP crystals in the coatings are rod-like in shape with a length of ~15 μm as shown in Figure 6(a). Added yttrium promotes lateral intergrowth of crystals for creating a dense film. For example, the width of crystals without the yttrium addition is less than 2 μm, while those with 0.067 M yttrium are up to 6 μm, as observed in Figure 6(a),(b). This is possibly due to the strong adsorption affinity of yttrium ions to c-surfaces promoting growth of wider crystals. A study of hydroxyapatite doped with various ions has shown that Y-HAP can absorb a greater amount of calcium compared with both undoped and HAP substituted with other

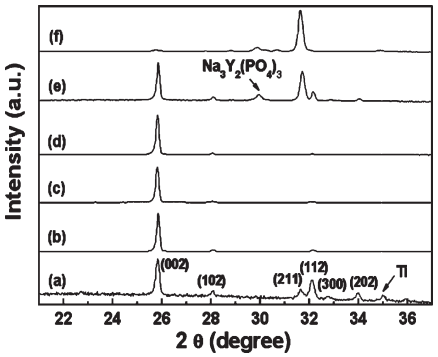

Figure 7. XRD patterns of HAP and Y-HAP coatings on titanium substrates: (a) HAP seeds, (b) HAP film without Y, (c) Y-HAP film with [Y] = 0.0067 M, (d) Y-HAP film with [Y] = 0.01 M, (e) Y-HAP film with [Y] = 0.02 M, and (f) Y-HAP film with [Y] = 0.05 M.

ions.[22] When starting yttrium content is less than 0.02 M, the obtained crystals are aligned and oriented with the *c*-axis normal to the substrate with the *c*-axis length greater than 10 μm, as shown in side view images in Figures 4(b) and 6(b). However, as [Y] was increased to 0.02 M, a remarkable morphology change in the coatings was observed. The films are ~2 μm thick, containing interconnected crystals with a well-defined hexagonal habit, but the c-axes of the hexagonal crystals are no longer vertically aligned, as shown in Figure 6(c),(d). For all samples shown in Figure 6, the initial pH was 10 and after the hydrothermal reaction it was ~9.7. The morphological changes in the Y-HAP coatings may result from the different positions of Y in the crystal framework when yttrium concentration is varied. There are two nonequivalent Ca sites available for cation substitution in an apatite unit cell. Ca(I) is positioned on the 3-fold axis and is surrounded by nine phosphate oxygen atoms, and Ca(II) is at the apex of staggered equilateral triangles surrounded by seven oxygen atoms.[26,31,34] It has been reported that at low doping levels the Y cations are randomly distributed among these two type sites, while at the high substitution levels, they go preferentially to the Ca(II) site.[26] The location of yttrium in the crystal framework will influence the growth rate of different facets to regulate the crystal morphology.

X-ray diffraction confirms the morphological changes observed by SEM, as shown in Figure 7. Figure 7(a) shows the diffraction pattern of the seed layer. The diffraction peaks from the seed layer are consistent with HAP, and no secondary phases were observed. The ratio of the intensities of the (002) to the (300) plane is quite large compared to the standard ratio of the random hydroxyapatite, which indicates a (002) (i.e., *c*-axis) preferred orientation normal to the substrate. Some HAP crystals are also oriented in other directions since several other diffraction peaks are still observed in Figure 7(a). This is in agreement with the cross-sectional observation as shown in Figure 1(b). After hydrothermal growth, the diffraction peaks are obviously sharper and stronger compared to the crystals in the seed layer, which suggests a higher degree of crystallization. The most notable feature of the pattern after hydrothermal growth is the enhancement in the intensity of the peak at 2θ of 25.8° which corresponds to the (002) reflection. The enhanced (002) intensity indicates that the c-axes of crystals are dominantly oriented normal to the substrate, consistent with the SEM observation in Figures 4(b), 6(a) and 6(b). The diffraction pattern in Figure 7(b) is consistent with the preferred crystal orientation of the sample

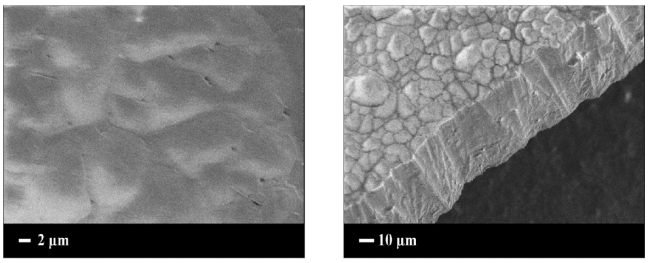

Figure 8. SEM images of fully dense Y-HAP coating on titanium prepared by electrochemical-hydrothermal method: (a) top-view image and (b) side-view image.

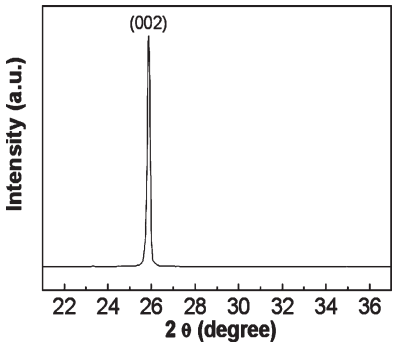

Figure 9. XRD pattern of fully dense Y-HAP coating on titanium prepared by electrochemical-hydrothermal method.

observed in Figure 6(a). When the starting [Y] is less than 0.02 M, the substitution of Y for Ca does not change the hexagonal crystal structure and no impurity is present, according to the XRD patterns of Figure 7(c),(d). However, as the Y concentration increased to 0.02 M, an enhancement in intensity of the (211) diffraction peak is observed in the pattern, indicating the crystals grow along the (211) direction normal to the substrate. This is also in agreement with the morphological changes as observed in Figure 6. The $Na_2Y_2(PO_4)_2$ phase appears in addition to the apatite phase when Y content is 0.02 M or greater, indicating that some excess Y^{3+} did not substitute in the apatite structure and reacted directly with PO_4^{3-}.

The effects of reagent concentrations, reaction time, and pH observed above were used as a guide to select conditions for growth of dense Y-HAP films. High calcium concentration and moderate yttrium concentration promotes lateral intergrowth of crystal domains, while high phosphate concentration promotes thicker films. Since growth kinetics slows after 15 h, the hydrothermal growth step was repeated using a synthetic solution containing 0.3 M $Ca(NO_3)_2$, 0.015 M $Y(NO_3)_3$, and 0.18 M $(NH_4)_2HPO_4$. Each growth step was carried out for 15 h at 200 °C with the starting pH of 10. After each step, the sample was taken out, rinsed with deionzed water and then placed into a new reactant solution to resume the hydrothermal reaction. The obtained Y-HAP coating appears as a uniform and strongly adherent layer on the substrate. The porosity of coatings decreased dramatically with repeated hydrothermal crystallization steps. After repeating the hydrothermal step three times, all crystal domains grow together to form a fully dense film with a thickness approximately 40 μm as shown in Figure 8. Analysis of

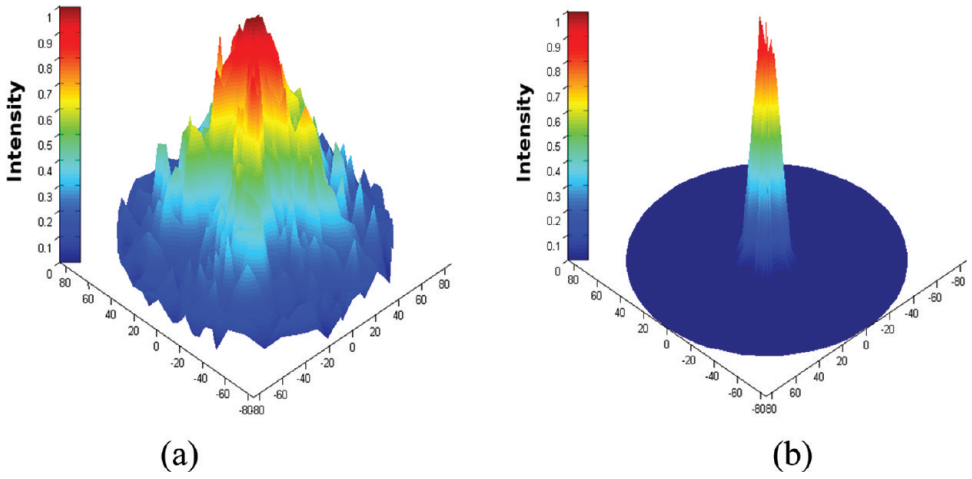

Figure 10. Pole figures of (002) peak of (a) seed layer shown in Figure 1 and (b) fully dense Y-HAP film shown in Figure 8. The tilt angle and rotation angle in degrees is plotted in Cartesian coordinates in the $x-y$ plane, while relative intensity of the (002) peak is plotted on the z-axis.

SEM images shows that the film porosity is approximately 20% after the first hydrothermal growth step, and porosity decreases to 0.4% after the third growth step. It should be noted that the porosity is likely overestimated because it was calculated from the fractional area occupied by crystals from the top-view SEM images. Side view images of fractured films show the porosity is lower at the base of the film in contact with titanium. The elemental composition of the dense film was probed with an energy dispersive X-ray spectrometer (Phoenix EDX) attached to the electron microscope. The EDX spectrum is composed of O, P, Ca, and Y peaks, confirming the presence of Y-HAP. Analysis of the EDX spectrum shows that the Ca/Y atomic ratio is around 12 in the film. The yttrium concentration is enhanced in the Y-HAP film relative to the starting synthesis solution that had a Ca/Y ratio of 20. The X-ray diffraction pattern of this film is shown in Figure 9. The only visible diffraction peak is from the (002) planes, indicating that all crystal domains are near perfectly aligned with the c-axis normal to the substrate.

Figure 10 shows three-dimensional pole figures of the (002) peak from the fully dense Y-HAP film shown in Figure 8 compared to that of the seed layer shown in Figure 1. The $x-y$ plane in Figure 10 is in Cartesian coordinates obtained by converting the polar coordinates of tilt angle and rotation angle in degrees. For a sample with perfect alignment of the c-axis normal to the substrate, the pole figure would appear as a point of maximum intensity at 0°, and falling to zero intensity as the sample is titled. The figure shows that the seed layer has preferential orientation of the c-axis normal to the substrate as the maximum intensity is centered around 0° of tilt angle. However, significant intensity from the (002) planes of the seed layer are measured at all tilt angles, indicating some fraction of the seed crystals are oriented normal to all tilt angles measured. In contrast, the fully dense film displays near perfect alignment of the c-axes normal to the substrate. For the fully dense Y-HAP coating, the intensity falls to zero for all tilt angles greater than ~20°. The results indicate that all crystal domains in the fully dense coating are oriented within ~20° of normal to the substrate. This is because the crystal growth in repeated reactions maintains the orientation of the original columnar crystals from the first hydrothermal reaction. The preferentially oriented crystal domains substantially span the film thickness so that no misaligned crystals are detected in the diffraction pattern.

The Y-HAP coatings are fairly durable and adherent to the titanium substrate. A fully dense film similar to the one shown in Figure 8 was subjected to the ASTM standard D3359 tape test. This test calls for a cross shape or hatch pattern to be cut into a coating with a sharp blade. Then, an adhesive tape (Elcometer 99) is applied across the coating and removed. The coating's adhesive strength is characterized qualitatively based on the amount of coating removed by the tape. The brittle nature of Y-HAP resulted in much of the film cracking and flaking as the cross shape was cut into the film with a razor. Essentially, all of the Y-HAP film was removed in the area cut by the blade before the tape could be applied. However, if the Elcometer 99 tape was applied to the as-synthesized fully dense Y-HAP film, none of the film was lost when the tape was removed. The results show that the Y-HAP coating adheres strongly to the metal, but can be easily damaged by cutting due to brittle fracture. Continuous and durable Y-HAP films on titanium can be potentially useful for load bearing orthopedic implants, particularly considering the enhanced osteoblast adhesion on Y-HAP compared with pure HAP.[22] The crystal orientation in the novel Y-HAP coatings is also ideal for electrically polarizing the crystal surfaces to further promote bone growth, and for promoting proton transport through the membrane.[27] Unfortunately, the novel Y-HAP films do not have porosity that is desirable in biomedical ceramic implants for promoting infiltration of surrounding tissue to obtain strong bioadhesion. Future work is needed to determine if the novel Y-HAP film structure reported here will prove advantageous in biomedical implants.

CONCLUSIONS

Yttrium substituted hydroxyapatite films on titanium were produced by electrochemical seeding followed by hydrothermal crystal growth. The method includes an electrochemical reaction to seed the metal substrate with a thin layer of HAP crystals and then a hydrothermal process to grow the Y-HAP coatings with a dense coverage onto the seeded substrates. The effects of several parameters such as reaction time, solution pH, and composition of the reactants were investigated in the hydrothermal process. A solution pH of 10 and hydrothermal reaction time of at least 15 h are favorable for growing dense and well crystallized Y-HAP coatings. Increasing phosphate concentration relative to calcium

increases coating thickness, while increasing calcium concentration relative to phosphate promotes dense surface coverage. The effect of yttrium concentration is complex, with moderate concentration promoting dense films with (002) orientation normal to the substrate and higher concentration promoting (211) orientation normal to the substrate. Hydrothermal reaction conditions were found that allow complete and uniform coating of Y-HAP onto titanium with near perfect alignment of the c-axes of crystal domains normal to the substrate through repeated hydrothermal crystallization steps. The preferred crystal orientation will facilitate proton transport through the coating thickness, potentially allowing improved performance of polarized films in orthopedic applications and as ion conducting membranes in electrochemical devices.

AUTHOR INFORMATION

Corresponding Author

*Tel: 1-585-273-2335; fax: 1-585-273-1348; e-mail: myates@che.rochester.edu.

ACKNOWLEDGMENT

We acknowledge NSF (CMMI-0856128), the DOE through the Laboratory for Laser Energetics (DE-FC03-92SF19460) and the University of Rochester for supporting this research.

REFERENCES

(1) Suchanek, W.; Yoshimura, M. *J. Mater. Res.* **1998**, *13*, 94–117.
(2) Nelea, V.; Morosanu, C.; Iliescu, M.; Mihailescu, I. N. *Appl. Surf. Sci.* **2004**, *228*, 346–356.
(3) Yang, Y.; Kim, K.-H.; Ong, J. L. *Biomaterials* **2005**, *26*, 327–337.
(4) Ban, S.; Maruno, S. *J. Biomed. Mater. Res.* **1998**, *42*, 387–395.
(5) Cheang, P.; Khor, K. A. *J. Mater. Process. Technol.* **1995**, *48*, 429–436.
(6) Liu, D.-M.; Yang, Q.; Troczynski, T. *Biomaterials* **2002**, *23*, 691–698.
(7) Onder, A.; Osman, E.-A.; Sabri, A. *Surf. Coat. Technol.* **2008**, *202*, 2482–2487.
(8) Haders, D. J.; Burukhin, A.; Huang, Y. Z.; Cockayne, D. J. H.; Riman, R. E. *Cryst. Growth Des.* **2009**, *9*, 3412–3422.
(9) Xue, W.; Tao, S.; Liu, X.; Zheng, X.; Ding, C. *Biomaterials* **2004**, *25*, 415–421.
(10) Yamashita, K.; Kitagaki, K.; Umegaki, T. *J. Am. Ceram. Soc.* **1995**, *78*, 1191–1197.
(11) Gittings, J. P.; Bowen, C. R.; Dent, A. C. E.; Turner, I. G.; Baxter, F. R.; Chaudhury, J. B. *Acta Biomater.* **2009**, *5*, 743–754.
(12) Tanaka, Y.; Nakamura, M.; Nagai, A.; Toyama, T.; Yamashita, K. *Mater. Sci. Eng. B Adv. Funct. Solid State Mater.* **2009**, *161*, 115–119.
(13) Maiti, G. C.; Freund, F. *J. Chem. Soc.-Dalton Trans.* **1981**, 949–955.
(14) Nakamura, S.; Takeda, H.; Yamashita, K. *J. Appl. Phys.* **2001**, *89*, 5386–5392.
(15) Nakamura, S.; Kobayashi, T.; Nakamura, M.; Yamashita, K. *J. Mater. Sci. - Mater. Med.* **2009**, *20*, 99–103.
(16) Itoh, S.; Nakamura, S.; Nakamura, M.; Shinomiya, K.; Yamashita, K. *Biomaterials* **2006**, *27*, 5572–5579.
(17) Nakamura, S.; Kobayashi, T.; Yamashita, K. *J. Biomed. Mater. Res.* **2002**, *61*, 593–599.
(18) Baxter, F. R.; Bowen, C. R.; Turner, I. G.; Dent, A. C. E. *Annal. Biomed. Eng.* **2010**, *38*, 2079–2092.
(19) Liu, D. X.; Savino, K.; Yates, M. Z. *Adv. Funct. Mater.* **2009**, *19*, 3941–3947.
(20) Lai, Z.; Bonilla, G.; Diaz, I.; Nery, J. G.; Sujaoti, K.; Amat, M. A.; Kokkoli, E.; Terasaki, O.; Thompson, R. W.; Tsapatsis, M.; Vlachos, D. G. *Science* **2003**, *300*, 456–460.
(21) Liu, D.; Savino, K.; Yates, M. Z. *Surf. Coat. Technol.* **2011**, *205*, 3975–3986.
(22) Webster, T. J.; Ergun, C.; Doremus, R. H.; Bizios, R. *J. Biomed. Mater. Res.* **2002**, *59*, 312–317.
(23) Sato, M.; Sambito, M. A.; Aslani, A.; Kalkhoran, N. M.; Slamovich, E. B.; Webster, T. J. *Biomaterials* **2006**, *27*, 2358–2369.
(24) Owada, H.; Yamashita, K.; Umegaki, T.; Kanazawa, T.; Nagai, M. *Solid State Ionics* **1989**, *35*, 401–404.
(25) Yamashita, K.; Owada, H.; Umegaki, T.; Kanazawa, T.; Katayama, K. *Solid State Ionics* **1990**, *40−1*, 918–921.
(26) Laghzizil, A.; Bouhaouss, A.; Barboux, P.; Morineau, R.; Livage, J. *Solid State Ionics* **1993**, *67*, 137–143.
(27) Wei, X.; Yates, M. Z. *Chem. Mater.* **2011**submitted.
(28) Ban, S.; Hasegawa, J. *Biomaterials* **2002**, *23*, 2965–2972.
(29) Zhang, H; Li, S.; Yan, Y. *Ceram. Int.* **2001**, *27*, 451–454.
(30) Kawasaki, T.; Niikura, M.; Kobayashi, Y. *J. Chromatogr.* **1990**, *515*, 125–148.
(31) Orlovskii, V. P.; Barinov, S. M. *Russ. J. Inorg. Chem.* **2001**, *46*, S129–S149.
(32) Berkovitchyellin, Z.; Vanmil, J.; Addadi, L.; Idelson, M.; Lahav, M.; Leiserowitz, L. *J. Am. Ceram. Soc.* **1985**, *107*, 3111–3122.
(33) Murphy, C. J. *Science* **2002**, *298*, 2139–2141.
(34) Ergun, C. *J. Eur. Ceram. Soc.* **2008**, *28*, 2137–2149.